Electronic Supplementary Material

Critical adhesion areas of cells on micro-nanopatterns

Shuang Zheng[1], Qiong Liu[1,2], Junhao He[1], Xinlei Wang[1], Kai Ye[1], Xuan Wang[1], Ce Yan[1], Peng Liu[1,3], and Jiandong Ding[1] (✉)

[1] *State Key Laboratory of Molecular Engineering of Polymers, Department of Macromolecular Science, Fudan University, Shanghai 200438, China*

[2] *Navy Characteristic Medical Center, the Second Military Medical University, Shanghai 200433, China*

[3] *College of Bioengineering, Chongqing University, Chongqing 400044, China*

Supporting information to https://doi.org/10.1007/s12274-021-3711-6

SUPPLEMENTARY MATERIALS AND METHODS

Details of fabrication of micro-nanopatterns

We put forward a hybrid patterning technique to elaborately control the RGD nanospacing and microisland size. In the present study, we fabricated micro-nanopatterns based on RGD nanopatterning. Such a nanotechnique employed block copolymer micelle nanolithography, and the main steps to fabricate nanopatterns are shown in Fig. 2(a) in the main manuscript. It was originally suggested by Spatz and Möller et al. for cell studies [S1], and has been developed to investigate cell adhesion and differentiation etc. by some groups including ours [S2-S4].

First, the block copolymer of poly(styrene-*block*-2-vinylpyridine) (PS-*b*-P2VP, Polymer Source) was dissolved in toluene, and gold precursor hydrogen tetrachloroaurate (III) hydrate ($HAuCl_4 \cdot 3H_2O$, Alfa Aesar) was dissolved in the above solution to form a micelle suspension. Then the micelle suspension was dip-coated onto a piece of clean and dry glass to form a self-assembled monolayer. After drying for 24 hours, oxygen plasma was applied to remove the block copolymer template. Ordered gold nanoarrays with different nanospacings can be obtained via various concentrations of block copolymers and dipcoating velocities etc. The fabrication parameters are listed in Table S1.

To prepare the microislands based on the glass slide with a pre-fabricated nanopattern, the glass modified with ordered gold nanoarrays was spin-coated with photoresist (RZJ-304, Suzhou Ruihong Electronic Chemicals Co. Ltd., China) and then selectively exposed to ultraviolet light (365 nm) covered with a designed micropattern mask. After treated by the corresponding developer, a photoresist micropattern was obtained on the top of a nanoarray. To etch the uncovered region, the patterned substrate was immersed in 0.5 mol/L HF/NH_4F buffer solution at 35 °C for 20 s twice. The regions not covered by the photoresist were etched off and simultaneously Au nanodots on these uncovered regions were removed together. Then the photoresist was lifted off by acetone, and a micropattern with Au nanodots sparsely arrayed inside individual microislands was generated on the glass substrate.

In order to provide a background without significant nonspecific cell adhesion, the glass substrate with micro-nanopatterns was immersed into a solution of linear PEG-silane (2-[methoxy(polyethyleneoxy)propyl] trimethoxysilane, namely, M-PEG-$Si(OMet)_3$). Finally, c(-RGDfK-)-thiol (f: D-phenylalanine, K: L-lysine; Peptides International) was used as the bridge between gold nanodots on the glass slide and integrins on the cell surface yet integrated into plasma membrane.

The micro-nanopatterns with different nanospacings were eventually achieved. Apart from the micro-nanopatterned surfaces, micropatterned surfaces were also prepared as the control group, which were fabricated by spraying gold onto photoresist-micropatterned glass slides which were not pre-treated by nanopatterning technique, using the same mask as in fabrication of micro-nanopatterns. A sputter coater (SBC-12, KYKY, China) was employed, followed by homogeneous RGD grafting. We designed a mask with round microdomains having diameters from 10 μm to 80 μm. The mask design and details of each repeating unit are shown in Fig. 3(a).

SUPPLEMENTARY RESULTS

Fabrication of micro-nanopatterns.

We fabricated micro-nanopatterns after combining top-down and bottom-up approaches and also HF etching. The etching led to a topographic morphology as demonstrated in Fig. S1.

Address correspondence to jdding1@fudan.edu.cn

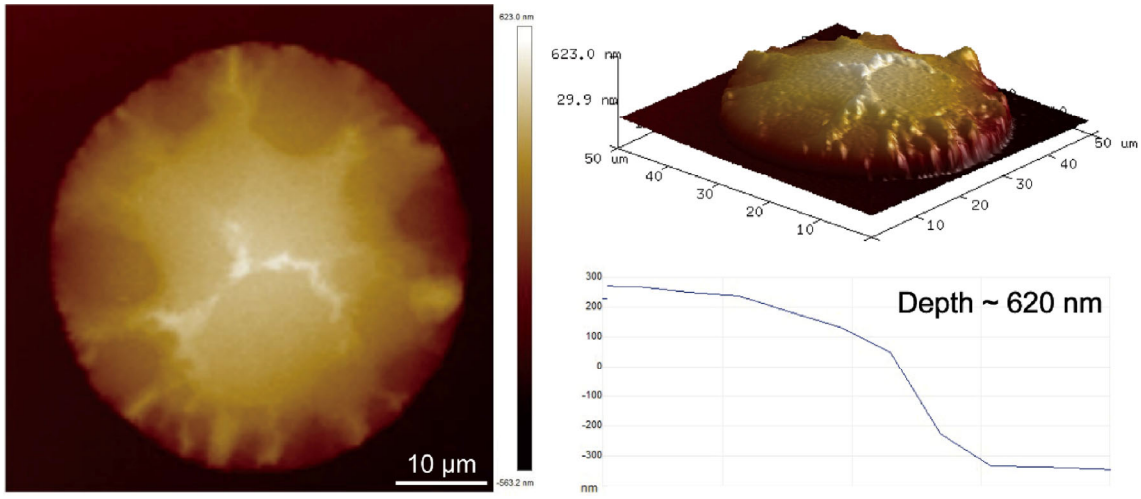

Figure S1 Microscopic observations of micro-nanopatterns by atomic force microscopy (AFM). The scanning area of this micrograph corresponds to 50 μm × 50 μm.

Selective adhesion or localization of hMSCs on nanoarrayed microislands with non-fouling background.

To verify the selectively adhesive property of the RGD micro-nanopatterns on the nonfouling PEG-monolayer-coated substrate, human mesenchymal stem cells (hMSCs) were seeded on the patterned surfaces with various microislands and nanospacings for 24 h and then immunofluorescently stained to show F-actins (red) and nuclei (blue). F-actins were stained in red fluorescence using phalloidin and cell nuclei were stained in blue using DAPI. Fig. 5 in the main manuscript demonstrates the excellent localization of stem cells inside the micro-nanoislands. The left is a schematic diagram of cell localization and the dipline crossing micro-nanoislands. The dipline indicated the boundary of the dip-coated region containing nanopatterns, proving successful fabrication of micro-nanopatterns for selective cell adhesion. The right fluorescence images show hMSCs adhering nearby the dipline, one is a merge image of F-actins and nuclei, and the other is a bright-field micrograph. With the excellent selectively adhesive property of our micro-nanopatterned surfaces, cells rarely passed across the dipline, and primarily occupied the modified region.

In addition, to confirm the long-term resistance of the non-fouling background to cell adhesion, hMSCs were seeded on nanopatterned surfaces with a PEG-coated background for 7 days. Typical fluorescence images of the counterstained cells on various micro-nanopatterns are shown in Fig. S2, where hMSCs were stained to show F-actins in red and nuclei in blue.

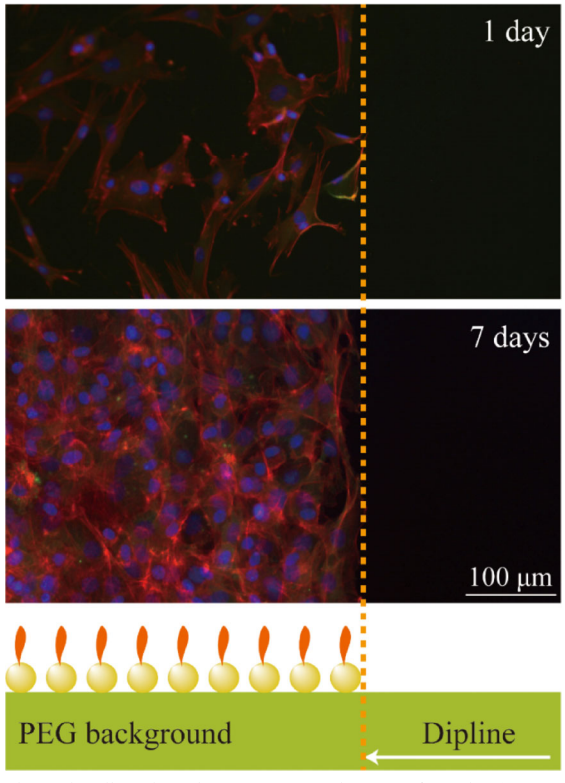

Figure S2 Fluorescence images of hMSCs selectively adhered on the nanopatterned regions for 1 day (upper image) and 7 days (lower image). The dashed line represents the dipline formed during dipcoating in fabrication of the nanopattern via block copolymer nanolithography. On the left side of the dipline, the RGD nanopattern was well organized atop a PEG background, while the right side of the dipline was merely the PEG background. The excellent anti-fouling efficacy of the self-assembled monolayer of PEG was well demonstrated, and the RGD nanopattern was confirmed to promote specific cell adhesion.

Four adhesion cases of cells on micro-nanopatterns are shown in Fig. S3. The hMSCs adhered only inside the micro-nanodomain with approximately round shape, wherein the circular micro-nanoislands have diameters of 40 μm and 80 μm & RGD nanospacings of 30 nm and 126 nm. We can see distinct adherent difference between microisland diameters and nanospacings. Cell occupied most of nanoarrayed microislands with diameter of 80 μm and nanospacing of 30 nm, whereas for nanoarrayed microislands having nanospacing of 126 nm only half of the nanoarrayed microislands were occupied by cells. The adherent cell number on the microislands of 80 μm-diameter was obviously more than that of 40 μm-diameter with the same nanospacing. In the lower right of this figure, there were barely cells localized on micro-nanoislands with 40 μm-diameter and 126 nm nanospacing.

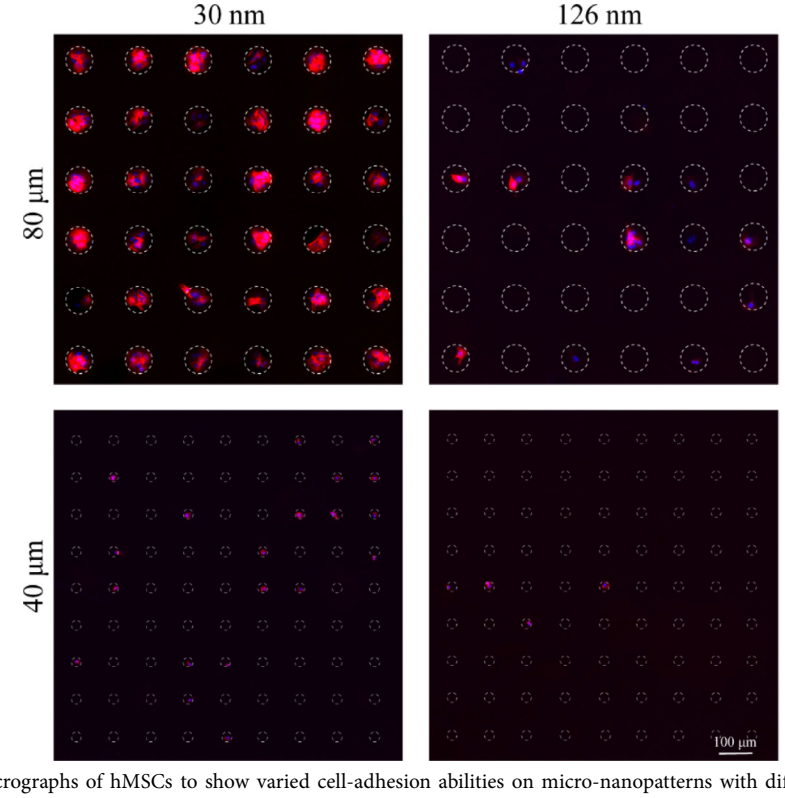

Figure S3 Fluorescence micrographs of hMSCs to show varied cell-adhesion abilities on micro-nanopatterns with different microisland sizes and/or different RGD nanospacings with the indicated two nanospacings and two microisland diameters as demonstration. The adherent hMSCs were stained to show F-actins in red and nuclei in blue.

Statistics of critical adhesion areas of hMSCs on nanoarrayed microislands with non-fouling background.

We define a micro/nanoisland with either one cell or multiple cells as "occupied". The percentage of occupied islands among all statistical microisland units gives the occupation fraction $f_{N>0}$ (the subscript N indicating cell number). Some data are shown in Figs. S4-S6.

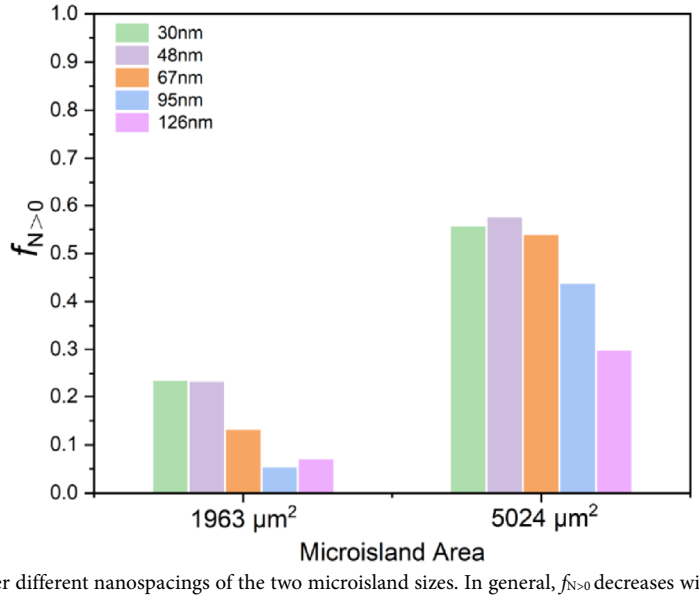

Figure S4 Histograms of $f_{N>0}$ under different nanospacings of the two microisland sizes. In general, $f_{N>0}$ decreases with the increase of RGD nanospacing under a given microisland size; $f_{N>0}$ increased with the increase of microisland size under a given RGD nanospacing.

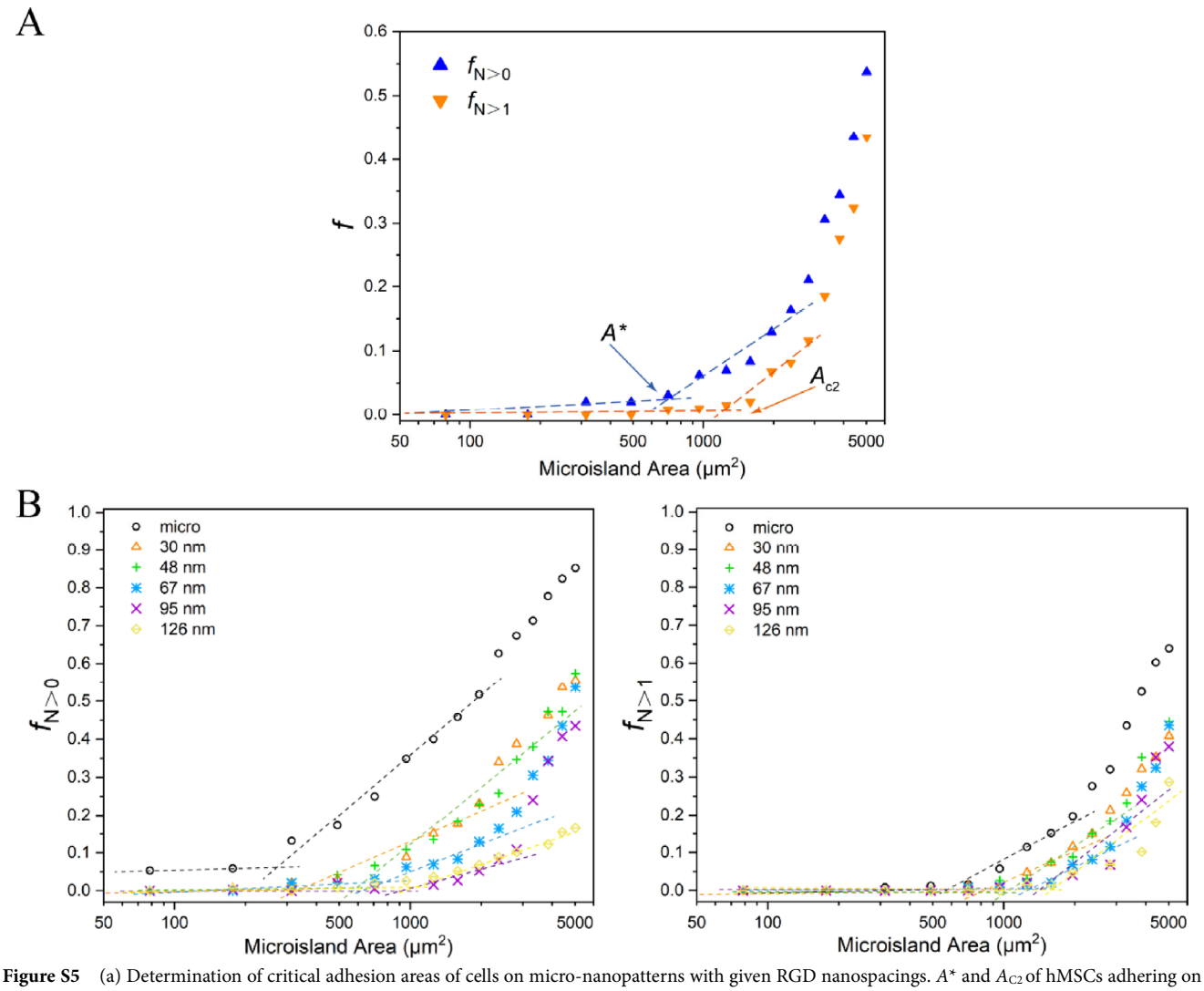

Figure S5 (a) Determination of critical adhesion areas of cells on micro-nanopatterns with given RGD nanospacings. A^* and A_{C2} of hMSCs adhering on micro-nanopatterns with 67 nm spacing as an example; (b) Left: fraction of cellular occupation per microisland ($f_{N>0}$) as a function of microisland area with the indicated nanospacings; Right: fraction of occupation of multiple cells per microisland ($f_{N>1}$) as a function of microisland area.

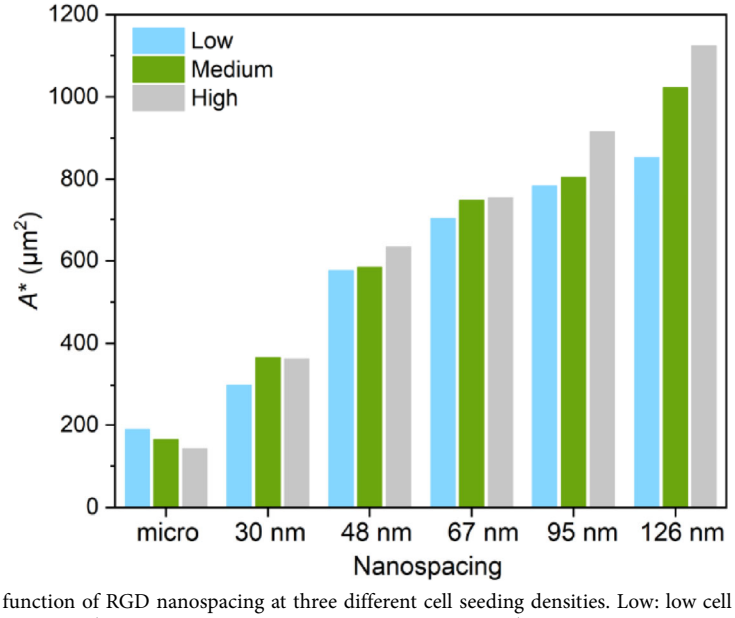

Figure S6 Critical area A^* as a function of RGD nanospacing at three different cell seeding densities. Low: low cell seeding density (2×10^4 cells/well); Medium: medium cell seeding density (4×10^4 cells/well); High: high cell seeding density (6×10^4 cells/well).

Statistics of cell densities and spreading areas under different RGD nanospacings and microisland sizes.

We also carried out statistics of adhesive cell density *versus* microisland size and nanospacing, as seem in Fig. S7.

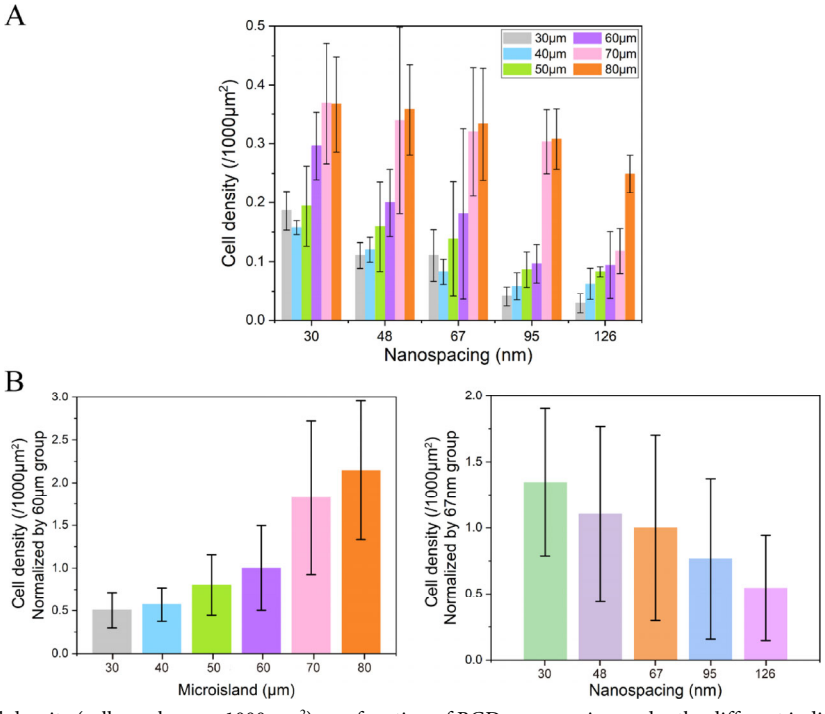

Figure S7 (a) Adhesive cell density (cell number per 1000 μm^2) as a function of RGD nanospacing under the different indicated microisland diameters; (b) Left: adhesive cell density as a function of microisland size normalized to the 60 μm-diameter group, $p = 1\times10^{-7}$, $n = 15$; Right: adhesive cell density as a function of nanospacing normalized to the 67 nm nanospacing group, $p = 2.14\times10^{-3}$, $n = 18$. The global test among all of the groups analyzed from one-way analysis of variance (ANOVA). The p-values obtained from one-way ANOVA are also listed in Tables S4 & S5.

We further compared average cell areas and single cell areas on 40 μm-diameter (left in Fig. S8) and 80 μm-diameter (right in Fig. S8) microislands with nanoarrays, where micro-nanoislands without cells were not included for statistics of cell area. On the micro-nanoislands with a small diameter of 40 μm, the average cell area and single cell area were relatively close, because only one cell can high probably adhere to small microislands. In contrast, the overall average cell area was larger than single cell areas on the large micro-nanoislands with a diameter of 80 μm, because large micro-nanoislands were prone to adhesion of multiple cells. With the increase of nanospacing, the average single cell area showed a significant reduction, owing to weak cell adhesion on microislands with nanoarrays of large RGD nanospacings such as 95 nm and 126 nm. The weak cell adhesion caused reduction of the average single cell area on micro-nanoislands and difficulty for cell spreading.

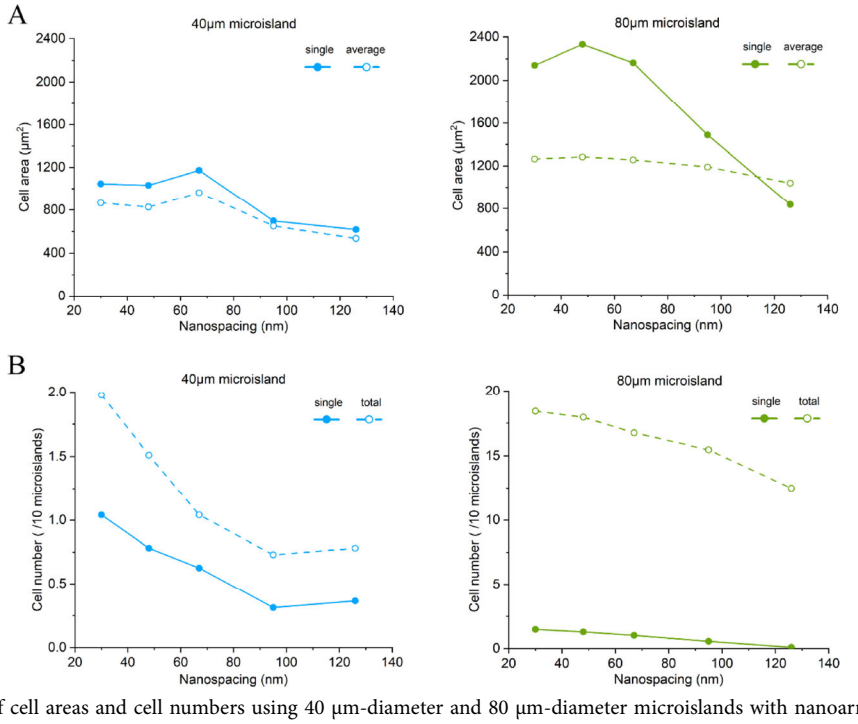

Figure S8 Comparison of cell areas and cell numbers using 40 μm-diameter and 80 μm-diameter microislands with nanoarrays as demonstration. (a) Average areas of all cells and average areas of single cells on 40 μm-diameter (left) and 80 μm-diameter (right) microislands. Those micro-nanoislands without cells were not included for statistics of cell area; (b) Total cell number and number of single cells on every 10 microislands of 40 μm-diameter (left) and 80 μm-diameter (right). All of micro-nanoislands with and without cells joined in statistics as denominator.

We also compared total cell number and single cell number at every 10 micro-nanoislands of 40 μm-diameter (left) and 80 μm-diameter (right), and micro-nanoislands with only one cell were included for statistics of single cell number. According to Fig. S8(b), the total cell number and the single cell number were relatively close on small micro-nanoislands with a diameter of 40 μm, and the cell number decreased with the increase of RGD nanospacing. Owing to multiple cell adhesion, the total cell number was much greater on large micro-nanoislands with a diameter of 80 μm than that on small microislands. Also, with the increase of RGD nanospacing, the cell number showed an evident decline.

Calculation of critical number of integrin-ligand binding N^*.

Here we define the number of binding between integrins and ligands as N, thus the critical number of integrin-ligand bonding is defined as N^*. The gold nanodots within micro-nanoislands is a hexagonal array. Accordingly, the area occupied by each gold nanodot a is correlated to the nanospacing D as

$$a = \frac{\sqrt{3}}{2} D^2 \tag{S1}$$

And the total number of nanodots N_{total} covered by a given cell area A reads

$$N_{total} = \frac{A}{a} = \frac{2A}{\sqrt{3}D^2} \tag{S2}$$

The calculated N_{total} as a function of nanospacing is shown in Fig. S9.

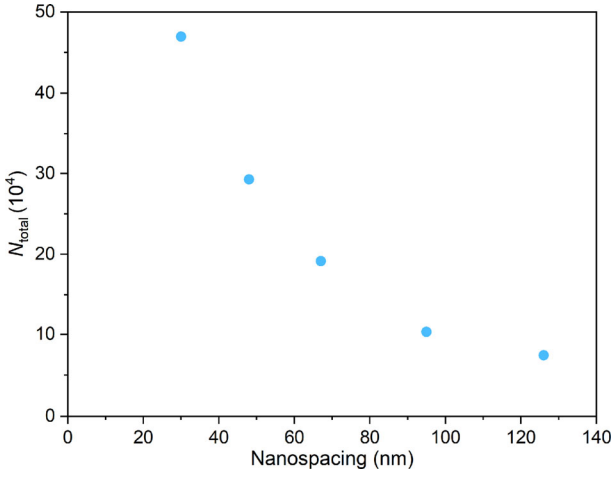

Figure S9 N_{total} as a function of RGD nanospacing.

The above formula implies our assumption that the total number of RGD binding sites within the critical adhesion area are consistent with the number of integrin binding sites. However, integrins were preferentially localized at the periphery of the adhesive island [S5-S7]. For membrane peeling, bond loading is highly nonuniform along the contact area: bond forces are maximal at the periphery and decay rapidly toward the center of a cell [S7]. The force for cell adhesion and morphology maintenance are mainly in the small areas at the cell edges, consistent with the distribution of integrins. Moreover, the most part of the bottom surface of a cell in contact with a material substrate does not contribute significantly to adhesion force [S6,S8,S9]. Therefore, the formula is further improved. We set the radius diameter of a circular micro-nanoisland as r and the average diameter of focal adhesion (FA) plaques as H, then the area of the outer ring with FA for cell adhesion on a micro-nanoisland reads

$$A = \pi r^2 - \pi(r - H)^2 = \pi H(2r - H) \tag{S3}$$

Accordingly, the number of gold nanodots corresponding to this critical region N^* is expressed as

$$N^* = \frac{2\pi H(2r - H)}{\sqrt{3}D^2} \tag{S4}$$

As is reported, the size of a FA plaque is 2 - 6 μm [S10,S11]. Under critical adhesion condition, cells were constrained to a restricted state so that the diameter of FA plaque H might be close to 2 μm. If we take H as 2 μm into equation (S4), there has an implicit condition that the amount of FA is constant for cells on microislands with nanoarrays of different RGD nanospacings.

The group of Andre´s J. Garcı´a [S8] found that integrin cluster and adhesive force are strongly modulated by the geometry of the nanoscale adhesive area. The minimal size of integrin-FN clusters required for FA assembly and force transmission exhibits an area threshold. Hence, we assumed that A^* depends on the effective adhesion area or on the effective ligand binding amount that can generate cell adhesion, that is to say, the number of FA plaques might be a constant. Then we brought H as 2 μm and $\pi = 3.14$ into equation (S4) and got the following formula:

$$N^* = 7.26\frac{d - 2}{D^2} \tag{S5}$$

Putting the data of the 5 groups of nanospacing into equation (S5), the resultant N^* as a function of nanospacing is shown in Fig. 9(b) in the main manuscript, which, however, does not exhibit a constant.

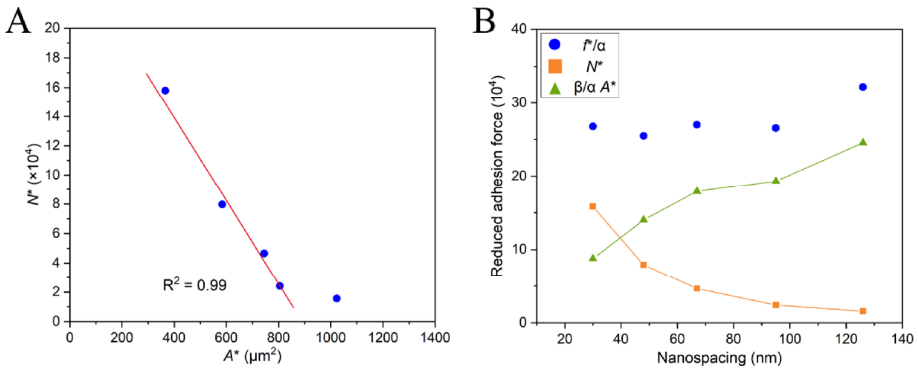

Figure S10 (a) The source of the coefficient of the calculation formula related to background adhesion, which as a function of critical adhesion area. The first four points were linearly fitted as $y = -0.03x + 26.24$; (b) Calculated adhesion force f on series of micro-nanoislands. According to $f^* = \alpha N^* + \beta A^*$, the reduced adhesion force reads $f^*/\alpha = N^* + \beta A^*/\alpha$.

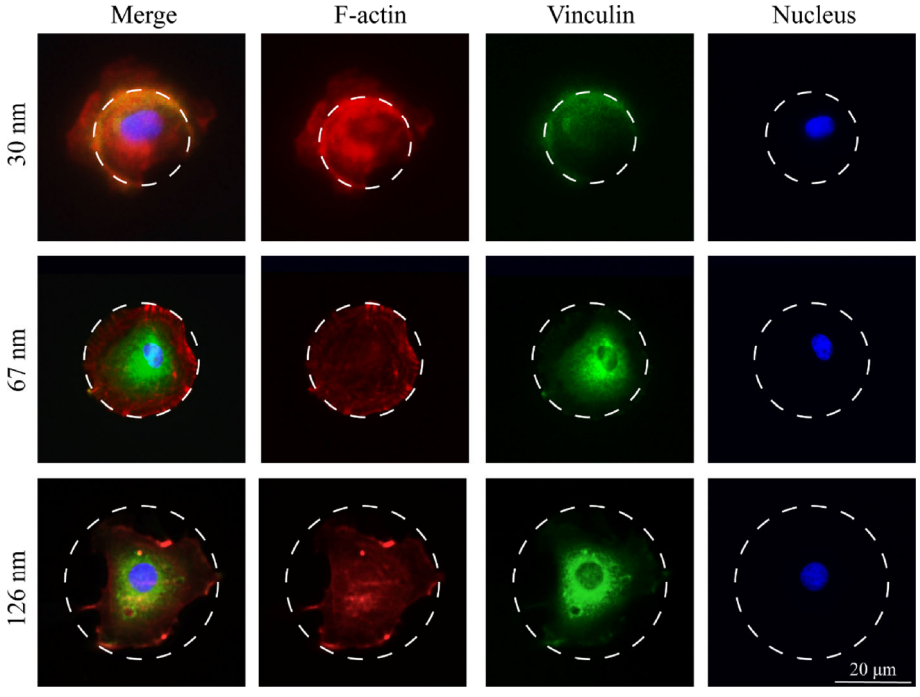

Figure S11 Fluorescence micrographs of single hMSCs on the indicated nanoarrayed microislands having a microisland size a bit larger than the corresponding critical adhesion areas. The adherent hMSCs were stained to show F-actin in red, vinculin in green and nucleus in blue.

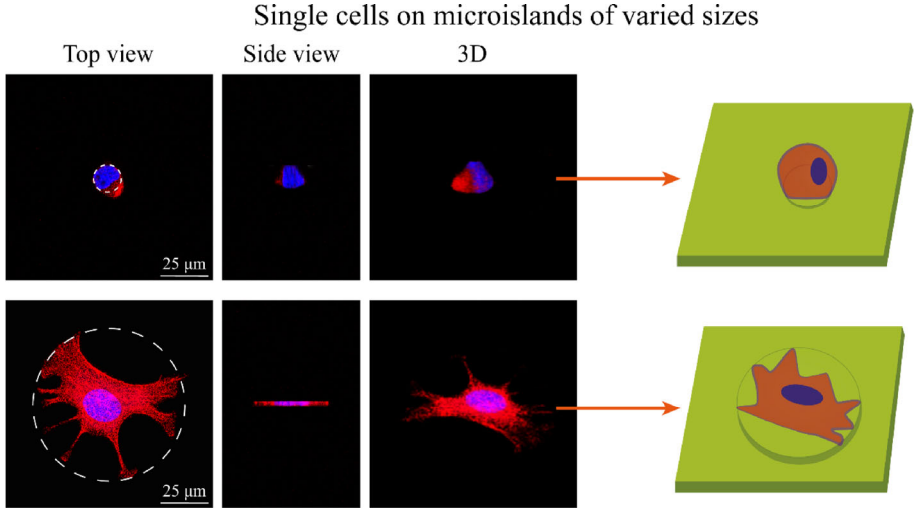

Figure S12 Single cells on microislands of the indicated two sizes. Here, the microislands in the absence of sparse nanoarrays were continuously sprayed with gold and densely grated with RGD ligands. The images were 3D reconstructed. The cells were stained to show F-actins in red and nuclei in blue.

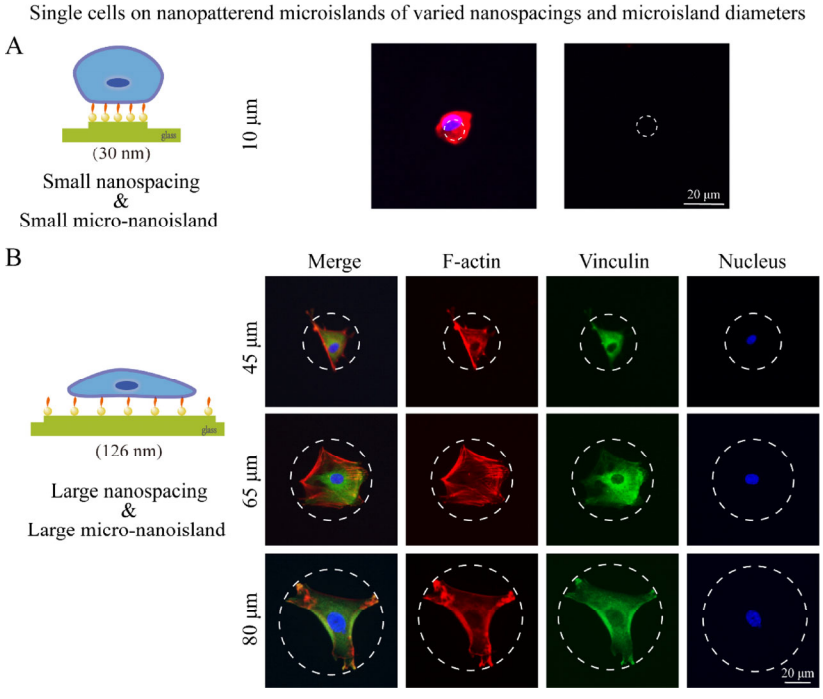

Figure S13 Single cells on nanopatterned microislands of the indicated different RGD nanospacings and microisland diameters. The adherent hMSCs were stained to show F-actins in red, vinculin in green and nuclei in blue. (a) Cells on 30 nm spaced micro-nanoisland with 10 μm-diameter: cells cannot adhere on this size of micro-nanoisland or can just spread beyond the microisland region; (b) Cells on 126 nm spaced micro-nanoisland with diameters of 45μm, 65μm and 80μm, respectively.

Table S1 Fabrication parameters of nanopatterns and the corresponding nanospacings of the micro-nanopatterns prepared in this study.

Block copolymer[a]	M_n	S unit: VP unit	Concentration[b] / mg·mL^{-1}	Loading amount[c]	Pulling speed[d] / μm·s^{-1}	Nanospacing[e] / nm
P18225	44300	320:105	7	0.6	200	30 ± 2
P4705	42500	288:199	7	0.6	200	48 ± 2
P4102	183500	1200:556	4	0.4	400	67 ± 5
P10851	188000	1296:504	3	0.4	400	95 ± 5
P5052	217000	1776:304	2	0.4	200	126 ± 6

[a] Block copolymer of poly(styrene-*block*-2-vinylpyridine) (PS-*b*-P2VP).

[b] Concentration of the block copolymer PS-*b*-P2VP in toluene.

[c] Loading amount of $HAuCl_4 \cdot 3H_2O$ in the block copolymer micelles, defined as the molar ratio of $HAuCl_4$ over that of 2-vinylpyridine blocks.

[d] Retracting velocity during dip-coating.

[e] Lateral spacing of the gold nanodots on glass.

Table S2 The *p*-values between groups of the middle image in Fig. 8(b) from one-way ANOVA.

p-value		Microisland diameter (μm)					
		30	40	50	60	70	80
Microisland diameter (μm)	30	--	0.840	0.241	0.004	0.036	0.000
	40	0.840	--	0.908	0.115	0.441	0.003
	50	0.241	0.908	--	0.633	0.962	0.058
	60	0.004	0.115	0.633	--	0.978	0.778
	70	0.036	0.441	0.962	0.978	--	0.331
	80	0.000	0.003	0.058	0.778	0.331	--

Table S3 The *p*-values between groups of the right image in Fig. 8(b) from one-way ANOVA.

p-value		Nanospacing (nm)				
		30	48	67	95	126
Nanospacing (nm)	30	--	0.968	1.000	0.014	0.000
	48	0.968	--	0.962	0.078	0.000
	67	1.000	0.962	--	0.013	0.000
	95	0.014	0.078	0.013	--	0.037
	126	0.000	0.000	0.000	0.037	--

Table S4 The *p*-values between groups of the left image in Fig. S7(b) from one-way ANOVA.

p-value		Microisland diameter (μm)					
		30	40	50	60	70	80
Microisland diameter (μm)	30	--	1.000	0.734	0.201	0.000	0.000
	40	1.000	--	0.888	0.350	0.000	0.000
	50	0.734	0.888	--	0.940	0.000	0.000
	60	0.201	0.350	0.940	--	0.003	0.000
	70	0.000	0.000	0.000	0.003	--	0.673
	80	0.000	0.000	0.000	0.000	0.673	--

Table S5 The *p*-values between groups of the right image in Fig. S7(b) from one-way ANOVA.

p-value		Nanospacing (nm)				
		30	48	67	95	126
Nanospacing (nm)	30	--	0.758	0.447	0.043	0.002
	48	0.758	--	0.987	0.467	0.057
	67	0.447	0.987	--	0.776	0.176
	95	0.043	0.467	0.776	--	0.815
	126	0.002	0.057	0.176	0.815	--

Supplementary References

[S1] Spatz, J. P.; Roescher, A.; Möller, M. Gold Nanoparticles in Micellar poly(styrene)-*b*-poly(ethylene oxide) Films—Size and Interparticle Distance Control in Monoparticulate Films. *Adv Mater.* **1996**, 8, 337-340.

[S2] Glass, R.; Möller, M.; Spatz, J. P. Block Copolymer Micelle Nanolithography. *Nanotechnology.* **2003**, 14, 1153-1160.

[S3] Wang, X.; Ye, K.; Li, Z.; Yan, C.; Ding, J. Adhesion, Proliferation, and Differentiation of Mesenchymal Stem Cells on RGD Nanopatterns of Varied Nanospacings. *Organogenesis*. **2013,** 9, 280-286.

[S4] Ye, K.; Wang, X.; Cao, L.; Li, S.; Li, Z.; Yu, L.; Ding, J. Matrix Stiffness and Nanoscale Spatial Organization of Cell-Adhesive Ligands Direct Stem Cell Fate. *Nano Lett*. **2015**, 15, 4720-4729.

[S5] Lehnert, D.; Wehrle-Haller, B.; David, C.; Weiland, U.; Ballestrem, C.; Imhof, B. A.; Bastmeyer, M. Cell Behavior on Micropatterned Substrata: Limits of Extracellular Matrix Geometry for Spreading and Adhesion. *J. Cell Sci.* **2004,** 117, 41.

[S6] Gallant, N. D.; Michael, K. E.; García, A. J. Cell Adhesion Strengthening: Contributions of Adhesive Area, Integrin Binding, and Focal Adhesion Assembly. *Mol. Biol. Cell.* **2005,** 16, 4329-4340.

[S7] Legerstee, K.; Geverts, B.; Slotman, J. A.; Houtsmuller, A. B. Dynamics and Distribution of Paxillin, Vinculin, Zyxin and VASP Depend on Focal Adhesion Location and Orientation. *Sci. Rep.* **2019**, 9, 10460.

[S8] Coyer, S. R.; Singh, A.; Dumbauld, D. W.; Calderwood, D. A.; Craig, S. W.; Delamarche, E.; García, A. J. Nanopatterning Reveals an ECM Area Threshold for Focal Adhesion Assembly and Force Transmission That is Regulated by Integrin Activation and Cytoskeleton Tension. *J. Cell Sci.* **2012,** 125, 5110.

[S9] Stolarska, M. A.; Rammohan, A. R. Center or Periphery? Modeling the Effects of Focal Adhesion Placement During Cell Spreading. *PLoS One.* **2017,** 12, e0171430.

[S10] Jérôme, M. G.; Philippe, P.; Gabor, C.; Jost, W. L.; Jean-Jacques, M.; Hinz, B. Focal Adhesion Size Controls Tension-Dependent Recruitment of α-Smooth Muscle Actin to Stress Fibers. *J. Cell Biol*. **2006,** 172, 259-268.

[S11] Sniadecki, N. J.; Desai, R. A.; Ruiz, S. A.; Chen, C. S. Nanotechnology for Cell–Substrate Interactions. *Ann. Biomed. Eng.* **2006,** 34, 59-74.